Published in final edited form as:
Earth Planet Sci Lett. 2017 September 15; 474: 466–473. doi:10.1016/j.epsl.2017.06.052.

The ruthenium isotopic composition of the oceanic mantle

K.R. Bermingham* and **R.J. Walker**
Isotope Geochemistry Laboratory, Department of Geology, University of Maryland, College Park, MD 20740 USA

Abstract

The approximately chondritic relative, and comparatively high absolute m antle abundances of the highly siderophile elem ents (HSE), suggest that their concentrations in the bulk silicate Earth were primarily established during a final ~0.5 to 1% of "late accretion" to the mantle, following the cessation of core segregation. Consequently, the isotopic composition of the HSE Ru in the mantle reflects an amalgamation of the isotopic compositions of late accretionary contributions to the silicate portion of the Earth. Among cosm ochem ical materials, Ru is characterized by considerable mass-independent isotopic variability, making it a powerful genetic tracer of Earth's late accretionary building blocks. To define the Ru isotopic composition of the oceanic mantle, the largest portion of the accessible mantle, we report Ru isotopic data for materials from one Archean and seven Phanerozoic oceanic m antle domains. A sample from a continental lithospheric mantle domain is also examined. All samples have identical Ru isotopic compositions, within analytical uncertainties, indicating that Ru isotopes are well mixed in the oceanic mantle, defining a μ^{100}Ru value of 1.2 ± 7.2 (2SD). The only known meteorites with the same Ru isotopic composition are enstatite chondrites and, when corrected for the effects of cosmic ray exposure, mem bers of the Main Group and sLL subgroup of the lAB iron meteorite complex which have a collective CRE corrected μ^{100}Ru value of 0.9 ± 3.0. This suggests that materials from the region(s) of the solar nebula sampled by these m eteorites likely contributed the dominant portion of late accreted materials to Earth's mantle.

Keywords

ruthenium isotopes; oceanic mantle; late accretion; IAB iron meteorites

1. Introduction

Ruthenium is a highly siderophile element (Re, Os, Ir, Ru, Pt, Rh, Pd, Au) comprising seven stable isotopes (^{96}Ru = 5.54%; ^{98}Ru = 1.8 7 %; ^{99}Ru = 12.8 %; ^{100}Ru = 12.6 %; ^{101}Ru = 17.1 %; ^{102}Ru = 31.6%; ^{104}Ru = 18.6 %). There are two short-lived chronometers associated with Ru, ^{98}T c –^{98}Ru and ^{99}Tc –^{99}Ru ($t_{1/2}$ = 4.2 – 10 Myr and $t_{1\,2}$ = 0.21 Myr, respectively; Kobayashi et al., 1993), however, no evidence for the presence of Tc in the early Solar System has yet been d iscovered. The HSE are highly soluble in metallic phases and are,

*Corresponding author: kberming@umd.edu (K.R. Bermingham).

Appendix A. Supplementary material
Supplementary material related to this article can be found on-line at http://dx.doi.org/10.1016/j.epsl.2017.06.052.

therefore, characterized by very high metal-silicate partition coefficients under low pressure conditions ($D^{Met/Sil}$ > 10,000, where D refers to the concentration ratio of an element in liquid metal to liquid silicate; Kimura et al., 1974; Mann et al., 2012). As a result, the putative lunar formin g impact and associated final core segregation event likely largely stripped the bulk silicate Earth (BSE) of HSE (Touboul et al., 2015). The projected absolute abundances of HSE in the BSE, however, are only ~200 times lower than bulk CI chondrites abundances, and the HSE are in approximately chondritic relative abundances (Morgan, 1986; Becker et al., 2006). Additionally, the projected $^{187}Os/^{188}Os$ and $^{186}Os/^{188}Os$ ratios for the BSE are within the range defined by chondritic meteorites (where $^{187}Re \rightarrow {}^{187}Os$: $t_{1/2}$ = 42 Gyr, $^{190}Pt \rightarrow {}^{186}Os$: $t_{1/2}$ = ~490 Gyr; Morgan, 1985; Walker et al., 1997; Meisel et al., 2001; Brandon et al., 2006). These characteristics are not predicted from metal-silicate partitioning experiments, making it unlikely that the HSE budget of the BSE was established as a result of coreformation (Chou, 1978; Morgan, 1986; Becker et al., 2006). A more plausible scenario is that the HSE were added to the BSE during a late accretion phase, that is, after cessation of core formation by the accretion of ~0.5 to 1 wt.% of Earth's mass to the mantle, in the form of plan - etesimals with chondritic bulk composition (Kimura et al., 1974; Chou, 1978). Further, late accretion may have been dominated by the impact of several large projectiles (2500 – 3000 km in diameter) stochastically delivered and emulsified into the BSE (Bottke et al., 2010; Dahl and Stevenson, 2010). Recent studies based on N body simulations and Pt isotope constraints support the contention that late accretion played a dominant role in establishing the abundances of HSE in the mantle (Rubie et al., 2016; Creech et al., 2017).

Given the likely late accretionary origin of the HSE in the BSE, these elements are well suited to probing the characteristics of late accretionary impactors. For example, the $^{187}Os/^{188}Os$, $^{186}Os/^{188}Os$, and the relative abundances of the HSE estimated for the BSE are most similar to some enstatite chondrites (e.g., Meisel et al., 1996, 2001; Becker et al., 2006; Brand on et al., 2006). Formulating accurate and precise projections of BSE compositions from mantle and mantle-derived materials, however, requires accurate assessment of the effects of prior mantle processing, such as melting, crystallization, and metasomatism (e.g., Alard et al., 2000; Becker et al., 2006). These are inherently difficult variables to constrain, and thus, their associated uncertainties have led to substantial conjecture inthe projections of BSE compositions and the composition of late accreted materials (Lorand et al., 2009).

Ruthenium isotopes are an important additional tool for constraining the genetics of late accretionary contributions to the BSE. Here, the term "genetic" refers to the isotopic compositions of the primary nebular materials from which an object was built (Walker et al., 2015). The utility of Ru isotopes for genetic study of late accreted materials is based on the assumption that most of the Ru present in the BSE was added by late accretion, as well as the observation that Ru is isotopically highly heterogeneous among different meteorite groups, with $^{100}Ru/^{101}Ru$ ratios varying by up to 140 ppm among chondrites and achondrites (Chen et al., 2010; Fischer-Gödde et al., 2015; Fischer-Gödde and Kleine, 2017). The large, mass-independent isotopic variations, termed anomalies, are presumed to result from the incorporation of variable proportions of presolar components, which were produced via nucle-osynthetic reactions in stars (e.g., *s*-, *r*-, *p-p rocess*; Zinner, 1998), into planetary building blocks. This heterogeneity is aproduct of either a poorly homogenized

distribution of presolar materials in the disk, or from thermal processing of presolar material in the disk (e.g., Qin and Carlson, 2016). Nucleosynthetic Ru isotope anomalies observ ed in meteorite groups most likely reflect variable incorporation of *s*-process materials in the feeding zones of their respective parent bodies (Chen et al., 2010; Fischer-Gödde et al., 2015; Fischer-Gödde and Kleine, 2017). By comparing the Ru isotopic compositions of different meteorites with the isotopic composition of the terrestrial mantle, it should be possible to identify the dominant signature of late accretionary impactors.

To successfully apply genetic testing, precise determination of the Ru isotope compositions of both cosmochemical and terrestrial mantle endmembers is required. P resently, the Ru isotopic composition of the BSE is poorly constrained. Two prior studies have reported limited data for Phanerozoic materials sampling two mantle sources, the Shetland Ophiolite Complex and the Josephine Ophiolite Complex (Fischer-Gödde et al., 2015; Bermingham et al., 2016), and one study has reported Ru isotope composition data for a Bushveld chromitite (Fischer-Gödde and Kleine, 2017). To more fully investigate the Ru isotopic composition of the oceanic mantle, we report isotopic data for Archean and Phanerozoic materials which were collected from eight oceanic mantle reservoirs. One sample, which likely samples the continental lithospheric mantle (Guli; Malitch and Lopatin, 1997; Merkle et al., 2012), is also included. The Ru isotopic compositions of the IAB iron meteorite complex have previously been reported to match that of the BSE (e.g., Chen et al., 2010; Fischer-Gödde et al., 2015), however, it was subsequently suggested that some IAB iron meteorites had a distinct Ru isotopic composition from the BSE (Fischer-Gödde and Kleine, 2017). As a result, we also conduct a detailed examination of six meteorites from this complex.

2. Samples

Terrestrial samples were selected based on their Ru concentration, age, and location, and include three whole rock chromitites and ten Os-Ir-Ru alloy grains (Table 1). Chromitites (C1, C2, C3) were provided by B. O'Driscoll (University of Manchester) as hand samples (~10 g). These chromitites were collected from serpen - tinized chromitite seams in the Cliff area of the Shetland Ophiolite Complex (~492 Ma; Spray and Dunning, 1991). The chromitites are characterize d by high Ru concentrations (≈2 3 pp m) and a narrow range in $^{187}Os/^{188}Os$ (0.12922 ± 3, 2σ, n = 6; O'Driscoll et al., 2012). The Ru isotopic compositions of the chromitites likely reflect the composition of their source region given the restricted mobility of HSE during serpentinization, the chemically robust nature of chromite, and the high concentration of the HSE in these samples (O'Driscoll et al., 2012). Furthermore, the Cr contents of the samples indicate that they formed as a result of high melt/rock interactions, implying that they provide a well-averaged composition of the oceanic mantle from which the rocks originated.

Multiple Os-Ir-Ru alloy grains from nine different worldwide locations were also analyzed (Table 1). The grains were obtained from the Natural History Museum, London (UK), I. Puchtel (University of Maryland, USA), and K.N. Malitch (A.N. Zavaritsky Institute of Geology and Geochemistry, Russia). Osmium-iridium-ruthenium alloys are commonly found in association with ultramafic rocks. They normally occur as inclusions within minerals such as chromite, or as detrital grains in streambeds draining peridotitic terrains.

Such grains are commonly interpreted to form as the result of either the release and subsequent reduction of Os, Ir and Ru during alteration of sulfides contained in upper mantle rocks, or by direct precipitation in upper mantle magma chambers (e.g., Cabri et al., 1996; Peck et al., 1992). By either mechanism, the Ru isotopic compositions of these grains likely provide an accurate reflection of the isotopic composition of their mantle source regions, given their high resistance to modification by subsequent thermal events and moderate to very high Ru concentrations (1 −30 wt.%; Malitch, 2004; Malitch et al., 2011).

Samples examined here include three Os-Ir-Ru grains found in placer deposits near Port Orford, Oregon (USA). These grains are associated with the Josephine Ophiolite Complex (Walker et al., 2005). The $^{187}Os/^{188}Os$ ratios of these grains are consistent with the Os isotopic composition of chromitites sampled from the Josephine Creek, indicating formation in the Mesozoic upper mantle (~162 Ma; Walker et al., 2005). The grains have between 43–73 wt.% Os, 15–37 wt.% Ir, 5.8 – 15 wt.% Ru, and display homogeneous intra- and inter-sample $^{187}Os/^{188}Os$ ratios (T able 1).

One Os-Ir-Ru alloy grain each from Bald Hills and Savage River, Tasmania, Australia, were analyzed. Grains collected from these locations have ^{187}Os-isotopic model ages of ~130 Ma (Walker et al., 1997; Brandon et al., 1998). One grain from Yodda, Papua New Guinea was analyzed. Spatially related grains from this are a have ^{187}Os-isotopic model ages of ~80 Ma (Brandon et al., 2006). No information about HSE abundances of the Bald Hills, Savage River, or Yodda alloy grains is currently available. Two Os-Ir-Ru alloy grains from the Nizhny Tagil and Kushva regions in the Urals, Russia were analyzed. No information about HSE abundances or Re-Osisotope systematics of the Kushva alloy grain is currently available, however, laurite and Os-Ir-Ru grains alloys from the neighboring Nizhny Tagil massif have Os-isotope model ages of ~870 ± 50 Ma (Anikina et al., 2014; Tessalina et al., 2015).

Two bulk samples comprising several small (<500 μm) Os-Ir-Ru alloy grains were analyzed. One was collected from Quaternary sediments in an area of the Ingaringa River (prospecting line L-365, Fig. 2 in Merkle et al., 2012) associated with the Guli clinopyroxene-dunite massif of the Maimecha-Kotui Province in Polar Siberia, Russia (Malitch and Lopatin, 1997). Osmium-iridium-ruthenium alloys from this region typically have ^{187}Os-isotopic model ages ranging from 545 to 615 Ma and between 65–98 wt.% Os, 1–39 wt.% Ir, and 1–4 wt.% Ru, and may represent a rare example of continental lithospheric mantle material (Table 1; Malitch et al., 2002). The second bulk sample (B-1), was collected from the Evander Goldfield in the Witwatersrand Basin. Similar grains typically have Os isotopic model ages consistent with formation at 2.7 to 4.1 Ga and between 5 – 55 wt.% Ru (Table 1; Malitch and Merkle, 2004).

To provide a cosmochemical comparison to the terrestrial Ru isotope data, six IAB iron meteorite complex samples were examined. Small chunks of these meteorite s were obtained from the Smithsonian Institution National Museum of Natural History (US). The IAB iron meteorite complex comprises meteorites that are chemically and texturally distinct from magmatic iron meteorites (Wasson and Kallemeyn, 2002). The complex is divided into the Main Group (MG) and five subgroups which are classified based on their Au and Ni

contents (sLL, sLM, sLH, sHL, and sHH; where s = subgroup; first capital= low or high Au content; second capital= low, medium, or high Ni content; Wasson and Kallemeyn, 2002). We analyzed three samples from the main group (MG: Campo del Cielo, Hope, and Morasko) and three samples from the sLL subgroup (Bischtübe, Deport, and Toluca; Table 1) which likely originated from the same parent body via impact-generated melts ~3.5 Ma and ~5.4 Ma, respectively, after formation of the Solar System, based on chemical, and ^{182}W and Mo isotopic data (Wasson and Kallemeyn, 2002; Worsham et al., 2017).

3. Methods

The Ru purification chemistry and analytical methods are the same as those reported in Bermingham et al. (2016). A brief de-scription is provided here. The Os–Ir–Ru alloy grains required no preparation prior to digestion. Chromitite samples were cut into 2–3 g pieces using a *MK Diamond Products Inc*. water-cooled tile saw and the pieces were abraded using silicon carbide sandpa-per to remove visible saw marks. Samples were then ground to a powder using an agate mortar and pestle. Iron meteorites were cut into <1 g pieces using a distilled water-cooled *Leco "Vari-cut"* saw with a 12.7cm diamond wafering blade, avoiding fusion crust and rust patches. The cut surfaces were abraded using silicon carbide sandpaper and sonicated in *Milli-Q* water three times for 10min at a time, using fresh *Milli-Q* water at each stage.

Alloys and chromitites were digested at 240 °C for 48h in a 30:70 mixture of concentrated HCl and HNO3, sealed in Pyrex Car-ius tubes. Although not critical here, complete digestion of the samples was not achieved. Previous studies indicate that variable and incomplete dissolution of materials do not result in a shift in the measured Ru isotopic composition (Fischer-Gödde et al., 2015;Bermingham et al., 2016; Fischer-Gödde and Kleine, 2017). The iron meteorites were digested using 8 M HCl and complete digestion was achieved. For all materials, the HSE were isolated from the matrix using cation exchange chromatography. Ruthenium was subsequently purified following microdistillation techniques de-scribed in Bermingham et al. (2016). The yields for the chemistry were variable, ranging from 20–90%. Obtaining consistently high Ru yields during microdistillation is difficult because of the com-plex redox chemistry exhibited by this element. Despite efficient distillation of Ru being promoted by using a strong oxidant to ox-idize the Ru and a strong reductant to reduce the captured Ru in the trap solution, yields were variable from sample to sample (see Bermingham et al., 2016). Total analytical blanks (including fila-ment loading blank) were <1 ng, which is ≪1% of the total Ru measured for each sample here, and inconsequential for the re-ported data.

Ruthenium isotope compositional data were obtained using a *Thermo-Fisher Triton Plus* thermal ionization mass spectrometer, operated in negative polarity mode. This instrument was equipped with nine Faraday cups which were used to measure the seven Ru isotopes as trioxides (RuO_3^-) using a single static line measurement method. Instrumental mass fractionation was corrected using the exponential law with $^{99}Ru/^{101}Ru \equiv 0.745075$ as the rele-vant normalizing ratio (following Chen et al., 2010;Fischer-Gödde et al., 2015;Bermingham et al., 2016; Fischer-Gödde and Kleine, 2017). To describe isotopic

compositions, we use the μ notation, which corresponds to the deviation of the $^{x}Ru/^{101}Ru$ of a sample, relative to the average ratio measured for the repeated analysis of the standard for that analytical campaign, in parts per mil-lion:

$$\mu^{x}\mathrm{Ru}_{sample} = \left[\frac{(^{x}_{101}\mathrm{R\ \ u})_{sample}}{(^{x}_{101}\mathrm{R\ \ u})_{standerd}} - 1\right] \times 10^{6}$$

High purity oxygen was bled into the source chamber using a variable leak valve to promote formation of RuO_3^-. Isobaric ox-ide interferences which develop as a result of the ionization of Ru as RuO_3^- were corrected using equations developed for Ru (see Bermingham et al., 2016 and references therein). The reported data were reduced using one of two different reduction protocols. One protocol utilized an assumed oxygen isotopic composition (obtained from Nier, 1950) for oxide interference corrections, while the other protocol relied on the direct measurement of the oxy-gen isotopic composition ("Nier reduction method" and "measured oxygen reduction method", respectively; Bermingham et al., 2016). The latter reduction scheme became available approximately mid-way through the course of this study with the addition of a 10^{13} Ω resistor amplifier to the instrument used. This permitted direct in-run monitoring of the oxygen isotope compositions by measuring $^{104}Ru\ ^{18}O\ ^{16}O_2$.

The in-house Ru standard used in this study was an *Alfa Ae-sar Specpure*® plasma standard solution (1000 μg/ml, $RuCl_3$ in 20% HCl). Repeat measurements of this standard using the Nier reduction method generated external reproducibility for different measurement campaigns was from μ^{96}Ru ± 61.0, μ^{98} Ru ± 144, μ^{100} Ru ± 5.59, μ^{102} Ru ± 29.2, μ^{104} Ru ± 30.3(2SD) to μ^{96} Ru ± 83, μ^{98} Ru ± 142, μ^{100} Ru ± 9.19, μ^{102} Ru ± 21.9, μ^{104} Ru ± 30.8 (2SD). Using a measured oxygen isotope composition, the external reproducibility was μ^{96} Ru ± 139, μ^{98} Ru ± 276, μ^{100} Ru ± 5.48, μ^{102} Ru ± 86.1, μ^{104} Ru ± 98.6 (2SD) to μ^{96} Ru ± 124, μ^{98} Ru ± 247, μ^{100} Ru ± 7.45, μ^{102} Ru ± 71.9, μ^{104} Ru ± 80.0 (2SD). The significantly worse precision on ^{96}Ru, ^{98}Ru, ^{102}Ru, ^{104}Ru when using a measured oxygen isotope composition reflects an unaccounted for effect in the oxygen isotope correction scheme (Bermingham et al., 2016). Although this is not desired, this is not relevant to this study. As a result of lower precision being reached on $^{96}Ru/^{101}Ru$, $^{98}Ru/^{101}Ru$, $^{102}Ru/^{101}Ru$, $^{104}Ru/^{101}Ru$, the values cal-culated using the Nier reduction method are reported for these isotopes. For the $^{100}Ru/^{101}Ru$ ratio, the reduction protocol using an assumed oxygen composition obtained from Nier (1950) was applied if in-run measurement of oxygen was not available for use or (rarely) higher in-run precision was achieved using an assumed oxygen composition, resulting from lower signal strength. The reduction protocol which used a measured in-run measure-ment of oxygen compositions was normally preferred because this technique corrects for variability in oxygen isotope compositions during an analysis. The $^{100}Ru/^{101}Ru$ ratio is used to constrain the Ru composition of the oceanic mantle because it is the ra-tio measured to the highest precision here ($\mu^{100}Ru/^{101}$ Ru ± 5.48 to ±9.20, 2SD) and it displays the largest nucleosynthetic isotope variability in cosmochemical materials. The external precision for $^{100}Ru/^{101}Ru$ varied slightly (μ^{100} Ru ± 5.48 to ±9.20) between 7 measurement campaigns over 3 yr, thus, samples were referenced to the standard data collected within their respective analytical session.

4. Results

The isotope compositions (μ^{x}Ru) for terrestrial samples are re-ported in Table 2 and SM1. The average μ^{100}Ru value of all mantle samples is 1.2 ±7.2, where the uncertainty reflects an average of the 2SD of repeated analysis of the *Alfa Aesar* standard from each measurement campaign. Most samples were analyzed once, how-ever, six sample solutions were measured multiple times (n =2–7; Fig. 1) by loading purified Ru from a single digestion onto different filaments. The uncertainties for sample means, where n < 3, are reported as the 2SD of the standard, or the sample, whichever was greater. The uncertainties for sample means, where n ≥ 3, are reported as the 2SE associated with the multiple measurements of the sample. The Os–Ir–Ru alloy from Guli (a material which likely samples the continental lithospheric mantle) falls within this composition μ^{100}Ru=1.6 ±3.9(2SE). Given that continental lithospheric mantle is likely ultimately created from the oceanic mantle, the Ru isotopic composition of Guli is included in the calculation of the average Ru isotope composition of the oceanic mantle composition.

The μ^{x}Ru values for IAB iron meteorites are reported in Table 3 and SM2. These data are not corrected for effects from cosmic ray exposure (CRE). Two of the sample solutions were analyzed multiple times (n =2–3) by loading purified Ru from a single di-gestion onto different filaments, whereas the remaining samples were analyzed only once. The uncertainties for multiple analyses of individual samples, where n <3, are reported as the 2SD of the standard, or the sample, whichever was greater. The uncertainties for individual samples, where n ≥3, are the 2SE associated with the multiple measurements of the sample.

5. Discussion

5.1. The Ru isotopic composition of the oceanic mantle

Using Ru isotope data collected from the Archean and Phanero-zoic materials analyzed here, the aggregate μ^{100}Ru value of 1.2 ±7.2 for the oceanic mantle suggests that the Ru isotopic composition of the oceanic mantle may have been homogeneous for at least the second half of Earth history. The uniformity of Ru iso-tope composition of the oceanic mantle can be explained in one of two ways. First, it is possible that late accretionary materials were genetically homogeneous. If there was no genetic diversity among late accreted materials, then isotopic variability in the man-tle should not be expected. Previous studies have concluded that materials added during the final ~10% of accretion, compared to materials added during the final ~0.5wt.% of accretion, were ge-netically similar, and that these materials formed in the same nebular feeding zone (e.g., Dauphas et al., 2004). The strongest evidence for this is the observation that Earth plots at one end of a linear trend defined by nucleosynthetic isotopic variations in both Mo and Ru for iron and chondritic meteorites (Dauphas et al., 2004). The Mo budget of the mantle was likely largely established by core formation processes during the final ~10wt.% of Earth accretion. By contrast, the Ru budget of the mantle was likely es-tablished by the final ~0.5wt.% of accretion. Consequently, Earth's mantle should only plot on this trend if the Mo and Ru contained within it were genetically very similar (e.g., Dauphas et al., 2004).

There are, however, lines of evidence that do not support complete genetic uniformity during Earth's final ~10wt.% of accretion. For example, materials contributing to the Earth during the accre-tion of the final ~0.5–1wt.% of the Earth's mass to the mantle may have included water-and organic-rich materials (Rubie et al., 2011). These potentially chemically diverse materials would likely have possessed considerable genetic diversity, as reflected in the genetic diversity exhibited by different meteorite groups (e.g., water-and organic-rich carbonaceous chondrites are characterized by large depletions in μ^{100}Ru, as low as −140; Fischer-Gödde and Kleine, 2017). Furthermore, new Mo and Ru isotopic data collected for meteorites suggest that planetesimals do not define a perfect linear trend on the Mo–Ru cosmic correlation (Bermingham et al., 2017). This indicates that the Mo and Ru in the mantle may not have been derived from the same, genetically unique feeding zone as was originally proposed. Also, the final stages of late accretion, believed by some to be defined by a late heavy bombardment of the inner Solar System, included chemically, and presumably genetically diverse materials, as recorded in the diversity of HSE characteristics of lunar impact melt rocks created by basin-forming impacts (Walker et al., 2015). Finally, dynamical models for late stages of planetary accretion suggest the participation of sizable bodies that formed in different nebular feeding zones, and likely possessed different genetic signatures (Bottke et al., 2010). Collec-tively, these observations suggest that there may not have been genetic uniformity among late accreted materials.

Given that Ru isotopic heterogeneity imparted by the late ac-cretion of genetically diverse materials may have been present in the early mantle, the apparently uniform Ru isotopic composition of the oceanic mantle could indicate that any initial isotopic di-versity present in the mantle was convectively mixed away by the end of the Archean. This is consistent with mantle mixing models which suggest that initial isotopic heterogeneities present in short-lived systems would be stirred away by ~3.8–2.8 Ga ago, resulting from convective mixing (Jacobsen and Yu, 2015). An interpretation of homogenization of late accretionary genetic diversity through convective mixing, however, requires that the isotopic composition of some late accreted materials extend to positive μ^{100}Ru values in order to offset negative values. To date, no bulk cosmochemical materials with μ^{100}Ru >> 0 have been identified.

Although the Ru isotopic composition of the oceanic mantle appears to have been homogeneous since ~2.7 Ga, there may be terrestrial rocks that record genetic diversity in late accreted ma-terials to the mantle. For example, some early Archean rocks are characterized by isotopic variations in the ^{182}Hf–^{182}W short-lived radiogenic isotope system (Touboul et al., 2012). These hetero-geneities likely reflect chemical and isotopic fractionations created within the first ~100 Ma of Earth history. The long-term preser-vation of primordial mantle ^{182}W signatures in the rock record suggests that the genetic signatures of pre-late accretionary ma-terials may still be preserved in the mantle. Additionally, Rizo et al. (2016) and Mundl et al. (2017) reported ^{182}W isotopic anoma-lies in young flood and ocean island basalts. The survival of mantle domains bearing isotopic heterogeneities created during the first ~100Ma of Earth history evidently extends to the present. Early Earth rocks and some modern ocean island basalts may, therefore, be fertile grounds in the search for Ru isotopic heterogeneity in-corporated in the mantle prior to late accretion.

5.2. A cosmochemical match to the oceanic mantle?

Prior studies have reported that iron meteorites from the IAB complex have Ru isotopic compositions similar to the composition of Earth's mantle (Chen et al., 2010;Fischer-Gödde et al., 2015). To compare the Ru isotopic composition of the oceanic mantle with the meteorites, modifications to the Ru isotopic composi-tions of the meteorites resulting from CRE must first be removed (e.g., Fischer-Gödde et al., 2015). To do this, we applied a group correction to the data for the meteorites. Osmium was used as the CRE dosimeter because it is a HSE which does not show re-solvable nucleosynthetic effects among bulk iron meteorites, but possesses large neutron capture cross sections and resonance in-tegrals for some isotopes (Mughabghab, 2003;Walker, 2012). The μ^{189}Os value was used here because it displays the largest neutron capture effects, where μ^{189}Os corresponds to the deviation of the ^{189}Os/^{188}Os of a sample, relative to average isotope ratio calculated for the repeat analysis of the *Alfa Aesar* standard for that analytical campaign, in parts per million:

$$\mu^{189}\mathrm{Os}_{sample} = \left[\frac{\left(^{189}\mathrm{O}\ \ ^{188}\mathrm{s}\right)_{sample}}{\left(^{189}\mathrm{O}\ \ ^{188}\mathrm{s}\right)_{standerd}} - 1 \right] \times 10^6$$

The collective correction for CRE for the six meteorites was obtained by regressing the μ^{189}Os values *vs.* μ^{100} Ru values for the six meteorites, then taking the pre-exposure composition for μ^{100} Ru to be at the point of intersection of the resulting trend with μ^{189}Os = 0 (Fig. 2). The CRE corrected composition for μ^{96} Ru, μ^{98} Ru, μ^{102} Ru, and μ^{104} Ru are also obtained using this approach, however, these values are not as robust as that deter-mined for μ^{100} Ru because μ^{189} Os *vs.* μ^{96} Ru μ^{98} Ru, μ^{102} Ru or μ^{104} Ru define weak correlations (SM2). The Os isotope data used here were collected from the same digestion solutions as the Ru isotopes, thus obviating issues associated with variable CRE effects due to the depth dependence of neutron capture effects. The Os analytical protocol for isolation and purification and Os isotope data are reported in Worsham et al. (2017). The pre-exposure μ^{100} Ru composition of $\mathrm{IABM}_{\mathrm{G,SLL}}$ obtained is 0.9 ± 3.0. The uncertainty (2SD) for this μ^{100} Ru value (and μ^{96} Ru μ^{98} Ru, μ^{102} Ru, μ^{104} Ru) is defined as the extent of the error envelop at μ^{189} Os = 0for the trend obtained using the ISOPLOT program (Ludwig, 2003).

The CRE corrected μ^{100} Ru value of 0.9 ± 3.0 we obtain for the IAB MG-sLL iron meteorites is similar to, but slightly higher than the CRE corrected μ^{100} Ru value of −11 ±7 reported for four MG IAB iron meteorites by Fischer-Gödde and Kleine (2017). That study used μ^{196} Pt was used as the CRE dosimeter. The pre-exposure composition was similarly obtained by correlating the μ^{196} Pt *vs.* μ^{100} Ru compositions of individual meteorites, and projecting to a pre-exposure composition at μ^{196} Pt = 0. The small difference in corrected μ^{100} Ru values may be an effect of differences in analytical procedures utilized in each study. This is unlikely, however, as both studies report analytically identical compositions for the Ru isotopic composition of Shetland ophiolite complex chromitite C3 (μ^{100} Ru= −0.4 ± 1.3 vs. 4 ± 6; this study and Fischer-Gödde and Kleine, 2017, respectively). Alternatively, the difference in the CRE corrected μ^{100} $\mathrm{Ru}_{\mathrm{IAB}}$ compositions may reflect a non-identical correction for CRE effects by the Pt and Os dosimeters. The difference between the

dosimeter composition for Campo del Cielo (the only common meteorite between the studies), μ^{189} Os 4.0 ± 5.0 and μ^{196} Pt 20 ± 7, is not necessarily meaningful, as this offset in μ^{189} Os may reflect a difference in the depth of the sample analyzed from the surface of the larger body exposed to cosmic rays in space. A clear assessment of the cause for the difference in $\mu^{100}Ru_{IAB}$ will necessitate future analyses of the Ru isotopic composition of additional IAB iron meteorite samples which show no evidence for neutron capture-induced isotopic shifts.

Based on our new results, the $IAB_{MG,sLL}$ (μ^{100} Ru 0.9 ± 3.0) me-teorite group possesses an indistinguishable μ^{100} Ru isotopic composition from the oceanic mantle (μ^{100} Ru 1.2 ±7.2; Fig. 1). The other meteorite group that has been measured to have a μ^{100} Ru isotope composition which overlaps with the oceanic mantle is the enstatite chondrite meteorite group (μ^{100} Ru −8 ± 4; Fischer-Gödde and Kleine, 2017; Fig. 1). The compositional parity between the feeding zone(s) from which enstatite chondrites and $IAB_{MG,sLL}$ iron meteorites formed and the source of the late accreted Ru sampled by the oceanic mantle most likely suggests the feeding zone(s) for these meteorites and the dominant contributors to terrestrial late accretion were from a region of the solar nebula with the same Ru genetic isotopic composition.

The decrease in the magnitude of μ^{100} Ru isotope anomalies (carbonaceous> ordinary> enstatite chondrites) has been inter-preted to indicate a heliocentric zoning of Ru isotope anomalies, suggesting that inner Solar System material was the primary contributor to late accretion (Fischer-Gödde et al., 2015; Fischer-Gödde and Kleine, 2017). Characteristics of the CI group, however, are discordant with this thesis. These chondrites are among the least thermally modified carbonaceous chondrites, yet they possess the most similar Ru isotopic composition (Fischer-Gödde and Kleine, 2017) to the Earth. Furthermore, the heliocentric zoning interpre-tation assumes that this zoning in the nebula was present at the time the parent bodies were forming. This assumption may be in-appropriate because the primordial compositional gradient of the solar nebula is currently unknown (Fernández et al., 2015). There is evidence for extensive mixing in the disk from silicate dust grains from comet P/Wild2, which possess crystalline features that could only have been formed in high temperature environments, in addition to more than half of Fe-bearing silicates showing evidence of inner Solar System processing (Zolensky et al., 2006;Fernández et al., 2015). Departing from the assumption that he-liocentric zoning was present in the disk at the time of par-ent body accretion by incorporating mixing between the inner and outer disk into late accretionary dynamical models may also help to constrain the characteristics of late accretionary materials.

6. Conclusions

The Ru isotope compositions of nine global locations sampling the oceanic mantle are reported. Ruthenium isotopic compositions are uniform among these locations and define a μ100Ru value of 1.2 ± 7.2 (2SD). This composition is the same as the parent body for the $IAB_{MG,sLL}$ iron meteorites (μ^{100} Ru of 0.9 ±3.0) and enstatite chondrites. This may indicate that enstatite chondrites, the IAB iron meteorite complex, and the dominant bodies added to the mantle by late accretion shared a common feeding zone.

Supplementary Material

Refer to Web version on PubMed Central for supplementary material.

Acknowledgements

We thank K. Malitch (Zavaritsky Institute of Geology and Geo-chemistry Ural Branch of Russian Academy of Sciences) for sharing his expertise in Os–Ir–Ru alloy geochemistry with us and for providing us with samples. B. O' Driscoll (University of Manchester, UK), I.S. Puchtel (University of Maryland, USA), Robin Hansen (Natural History Museum in London, UK), and Tim McCoy (Smithso-nian Institute National Museum, US) are thanked for providing us with samples. We thank the editor F. Moynier and two anonymous reviewers for their thorough and constructive reviews. We also thank I.S. Puchtel and E.A. Worsham for helpful discussions. Funding for this work was provided by NSF EAR 1624587, NASA SERVII NNA14AB07A, NASA Emerging Worlds NNX16AN07G, and RFBR 15-05-08332-a.

References

Alard O, Griffin WL, Lorand J-P, Jackson SE, O'Reilly SY, 2000 Non-chondritic distribution of the highly siderophile elements in mantle sulphides. Nature 407, 891–894. [PubMed: 11057664]

Anikina EV, Malitch KN, Pushkarev EV, Shmelev VR, 2014 The Nizhny Tagil and Volkovsky Massifs of the Uralian Platinum Belt, and Related Deposits, Field Trip Guidebook. Russian Academy of Sciences, Zavaritsky Institute of Geology and Geochemistry

Becker H, Horan MF, Walker RJ, Gao S, Lorand J-P, Rudnick RL, 2006 Highly siderophile element composition of the Earth's primitive upper mantle: constraints from new data on peridotite massifs and xenoliths. Geochim. Cosmochim. Acta 70, 4528–4550.

Bermingham KR, Worsham EA, Walker RA, 2016 Refinement of high precision Ru isotope analysis using negative thermal ionization mass spectrometry. Int. J. Mass Spectrom 403, 15–26. [PubMed: 30713465]

Bermingham KR, Worsham EA, Walker RA, 2017 New insights into the genetics of planetary building blocks In: 48th Lunar and Planetary Science Conference.

Bottke WF, Walker RJ, Day JMD, Nesvorny D, Elkins-Tanton L, 2010 Stochastic late accretion to Earth, the Moon and Mars. Science 330, 1527–1530. [PubMed: 21148387]

Brandon AD, Walker RJ, Puchtel IS, 2006 Platinum-Os isotope evolution of the Earth's mantle: constraints from chondrites and Os-rich alloys. Geochim. Cosmochim. Acta 70, 2093–2103.

Brandon AD, Walker RJ, Morgan JW, Norman MD, Prichard HM, 1998 Coupled ^{186}Os-^{187} Os evidence for core-mantle interaction. Science 280, 1570–1573. [PubMed: 9616113]

Cabri L-J, Harris DC, Weiser TW, 1996 Mineralogy and distribution of platinum-group mineral (PGM) placer deposits of the world. Explor. Min. Geol 5, 73–167.

Chen JH, Papanastassiou DA, Wasserburg GJ, 2010 Ruthenium endemic isotope effects in chondrites and differentiated meteorites. Geochim. Cosmochim. Acta 74, 3851–3862.

Chou C-L, 1978 Fractionation of siderophile elements in the Earth's upper mantle In: Proc. Lunar Planet. Sci. Conf. 9th, pp. 219–230.

Creech J, Baker J, Handler M, Lorand J-P, Storey M, Wainwright A, Luguet A, Moynier F, Bizzarro M, 2017 Late accretion history of the terrestrial planets inferred from platinum stable isotopes. Geochem. Perspect. Lett 94 (104).

Dahl TW, Stevenson DJ, 2010 Turbulent mixing of metal and silicate during planet accretion and interpretation of the Hf-W chronometer. Earth Planet. Sci. Lett 295, 177–186.

Dauphas N, Davis AM, Marty B, Reisberg L, 2004 The cosmic molybdenumruthenium isotope correlation. Earth Planet. Sci. Lett 226, 465–475.

Fernández YR, Li J-Y, Howell ES, Woodney LM, 2015 Asteroids and Comets In: Schubert G (Ed.), Treatise on Geophysics, vol.10 Elsevier, Amsterdam, pp. 487–528.

Fischer-Gödde, Kleine T, 2017 Ruthenium isotopic evidence for an inner Solar System origin of the late veneer. Nature 541, 525–527. [PubMed: 28128236]

Fischer-Gödde M, Burkhardt C, Kruijer TS, Kleine T, 2015 Ru isotope heterogeneity in the solar protoplanetary disk. Geochim. Cosmochim. Acta 168, 151–171.

Jacobsen S, Yu G, 2015 Extinct isotope heterogeneities in the mantles of Earth and Mars: Implications for mantle stirring rates. Meteorit. Planet. Sci 50, 555–567.

Kimura K, Lewis RS, Anders E, 1974 Distribution of gold and rhenium between nickel-iron and silicate melts. Geochim. Cosmochim. Acta 38, 683–781.

Kobayashi T, Sueki K, Ebihara M, Nakahara M, Imamura M, Masuda A, 1993 Half-lives of technetium-97, technetium-98. Radiochim. Acta 63, 29–31.

Lorand J-P, Alard O, Godard M, 2009 Platinum-group element signature of the primitive mantle rejuvenated by melt-rock reactions: evidence from Sumail peridotites (Oman Ophiolite). Terra Nova 21,35–40.

Ludwig KR, 2003 User's Manual for Isoplot 3.00 Berkeley Geochronology Center Special Publication No. 4, Berkeley, CA, 70 pp.

Malitch KN, 2004 Osmium isotope constraints on contrasting sources and prolonged melting in the Proterozoic upper mantle: evidence from ophiolitic Ru-Os sulfides and Ru-Os-Ir alloys. Chem. Geol 208, 157–173.

Malitch KN, Lopatin GG, 1997 New data on the metallogeny of the unique Guli clinopyroxenite-dunite Massif, Northern Siberia, Russia. Geol. Ore Depos 39, 209–218.

Malitch KN, Merkle RKW, 2004 Ru-Os-Ir-Pt and Pt-Fe alloys from the Evander Goldfield, Witwatersrand Basin, South Africa: detrital origin inferred from compositional and osmium-isotope data. Can. Mineral 42, 631–650.

Malitch KN, Augé T, Badanina I.Yu., Goncharov MM, Junk SA, Pernicka E, 2002 Os-rich nuggets from Au-PGE placers of the Maimecha-Kotui Province, Russia: a multi-disciplinary study. Mineral. Petrol76,1–28.

Malitch KN, Badanina I.Yu., Kotoyanov AI, 2011 Initial Os-isotopic composition of Os-Ir-Ru alloys from ultramafic massifs of the Polar Siberia. Dokl. Earth Sci 440, 1343–1348.

Merkle RKW, Malitch KN, Grasser PPH, Badanina I.Yu, 2012 Native osmium from the Guli Massif, Northern Siberia (Russia). Mineral. Petrol 104, 115–127.

Mann U, Frost DJ, Rubie DC, Becker H, Audétat A, 2012 Partitioning of Ru, Rh, Pd, Re, Ir and Pt between liquid metal and silicate at high pressures and high temperatures - implications for the origin of highly siderophile element concentrations in the Earth's mantle. Geochim. Cosmochim. Acta 85, 593–615.

Meisel T, Walker RJ, Morgan JW, 1996 The osmium isotopic composition of the primitive upper mantle. Nature 383, 517–520.

Meisel T, Walker RJ, Irving AJ, Lorand J-P, 2001 Osmium isotopic compositions of mantle xenoliths: a global perspective. Geochim. Cosmochim. Acta 65, 1311–1323.

Morgan JW, 1985 Osmium isotope constraints on Earth's late accretionary history. Nature 317, 703–705.

Morgan JW, 1986 Ultramafic xenoliths: clues to Earth's late accretionary history. J. Geophys. Res 91,12,375–12,387.

Mughabghab SF, 2003 Thermal neutron capture cross sections resonance integrals and G-factors

Mundl A, Touboul M, Jackson MG, Day JMA, Kurz MD, Lekic V, Helz RL, Walker RJ, 2017 Tungsten-182 heterogeneity in modern ocean island basalts. Science 356, 66–69. [PubMed: 28386009]

Nier AO, 1950 A redetermination of the relative abundances of the isotopes of carbon, nitrogen, oxygen, argon, and potassium. Phys. Rev 77, 789–793.

O'Driscoll B, Day JMD, Walker RJ, Daly JS, McDonough WF, Piccoli PM, 2012 Chemical heterogeneity in the upper mantle recorded by peridotites and chromitites from the Shetland Ophiolite Complex, Scotland. Earth Planet. Sci. Lett 333–334, 226–237.

Peck DC, Keays RR, Ford RJ, 1992 Direct crystallization of refractory platinum-group element alloys from boninitic magmas: evidence from Western Tasmania. Aust. J. Earth Sci 39, 373–387.

Qin L, Carlson RW, 2016 Nucleosynthetic isotope anomalies and their cosmo-chemical significance. Geochem. J 50, 43–65.

Rizo H, Walker RJ, Carlson RW, Horan MF, Mukhopadhyay S, Manthos V, Francis D, Jackson MG, 2016 Preservation of Earth-forming events in the tungsten isotopic composition of modern flood basalts. Science 352, 809–812. [PubMed: 27174983]

Rubie DC, et al., 2011 Heterogeneous accretion, composition and core-mantle differentiation of the Earth. Earth Planet. Sci. Lett 301, 31–42.

Rubie DC, Laurenz V, Jacobson SA, Morbidelli A, Palme H, Vogel AK, Frost DJ, 2016 Highly siderophile elements were stripped from Earth's mantle by iron sulfide segregation. Science 353, 1141–1144. [PubMed: 27609889]

Spray JG, Dunning GR, 1991A U/Pb age for the Shetland Islands oceanic fragment, Scottish Caledonides: evidence from anatectic plagiogranites in 'layer 3' shear zones. Geol. Mag 128 (6), 667–671.

Tessalina SG, Malitch KN, Augé T, Puchkov VN, Belousova E, McInnes B, 2015 Origin of the Nizhny Tagil clinopyroxenite-dunite massif (Uralian Platinum Belt, Russia): insights from PGE and Os isotope systematics. J. Petrol 56, 2297–2318.

Touboul M, Puchtel IS, Walker RJ, 2012 ^{182}W evidence for long-term preservation of early mantle differentiation products. Science 335, 1065–1069. [PubMed: 22345398]

Touboul M, Puchtel IS, Walker RJ, 2015 Tungsten isotopic evidence for disproportional late accretion to the Earth and Moon. Nature 520, 530–533. [PubMed: 25855299]

Walker RJ, 2012 Evidence for homogeneous distribution of osmium in the protosolar nebula. Earth Planet. Sci. Lett 351, 36–44.

Walker RJ, Morgan JW, Smoliar MI, Beary E, Czamanske GK, Horan MF, 1997 Application of the ^{190}Pt-^{186}Os isotope system to geochemistry and cosmochemistry. Geochim. Cosmochim. Acta 61, 4799–4808.

Walker RJ, Brandon AD, Bird JM, Piccoli PM, McDonough WF, Ash RD, 2005 ^{186}Os-^{187}Os systematics of Os-Ir-Ru alloy grains, southwestern Oregon. Earth Planet. Sci. Lett 230, 211–226.

Walker RJ, Bermingham KR, Liu J, Puchtel IS, Touboul M, Worsham EA, 2015 In search of late-stage planetary building blocks. Chem. Geol 411, 125–142.

Wasson JT, Kallemeyn GW, 2002 The IAB iron-meteorite complex: a group, five subgroups, numerous grouplets, closely related, mainly formed by crystal segregation in rapidly cooling melts. Geochim. Cosmochim. Acta 66, 2445–2473.

Worsham E, Bermingham KR, Walker RJ, 2017 Characterizing cosmochemical materials with genetic affinities to the Earth: genetic and chronological diversity within the IAB iron meteorite complex. Earth Planet. Sci. Lett 467, 157–166. [PubMed: 30713346]

Zinner E, 1998 Stellar nucleosynthesis and the isotopic composition of presolar grains from primitive meteorites. Annu. Rev. Earth Planet. Sci 26, 147–188.

Zolensky ME, et al., 2006 Mineralogy and petrology of comet 81P/Wild 2 nucleus samples. Science 314, 1735–1739. [PubMed: 17170295]

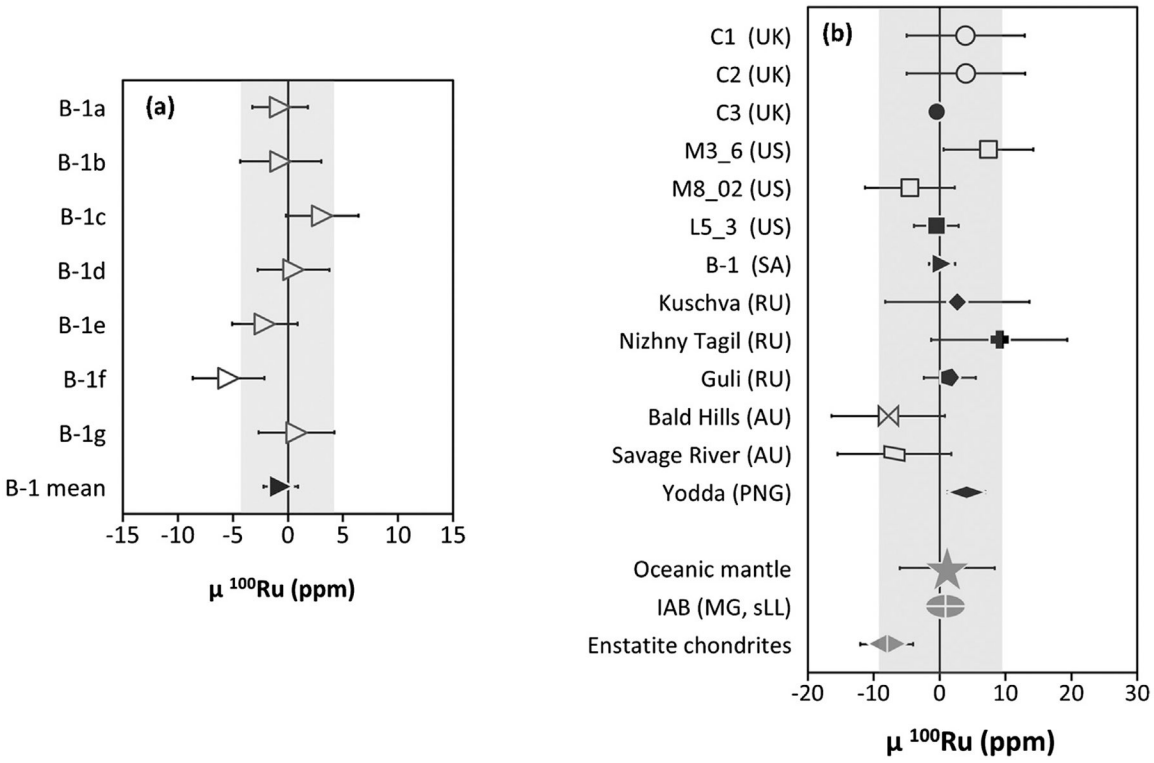

Fig. 1.

μ^{100} Ru for (a) repeat analyses of Ru-Os-Ir alloy B-1 from Witwatersrand, SA; and (b) Shetland Ophiolite Complex chromitites, Os-Ir-Ru alloys, oceanic mantle, CRE corrected $IAB_{mg,sLL}$, and enstatite chondrite group average (from Fischer-Gödde and Kleine, 2017). Filled symbols represent the mean of multiple analyses of the sample. The oceanic mantle composition is the average μ^{100} Ru composition and the uncertainty reflects an average of the 2SD of repeated analysis of the *Alfa Aesar* standard from each measurement campaign. The grey fields represent the 2SD of the standards measured during the relevant analytical campaigns. The lowest precision achieved during an analytical session displayed in (b).

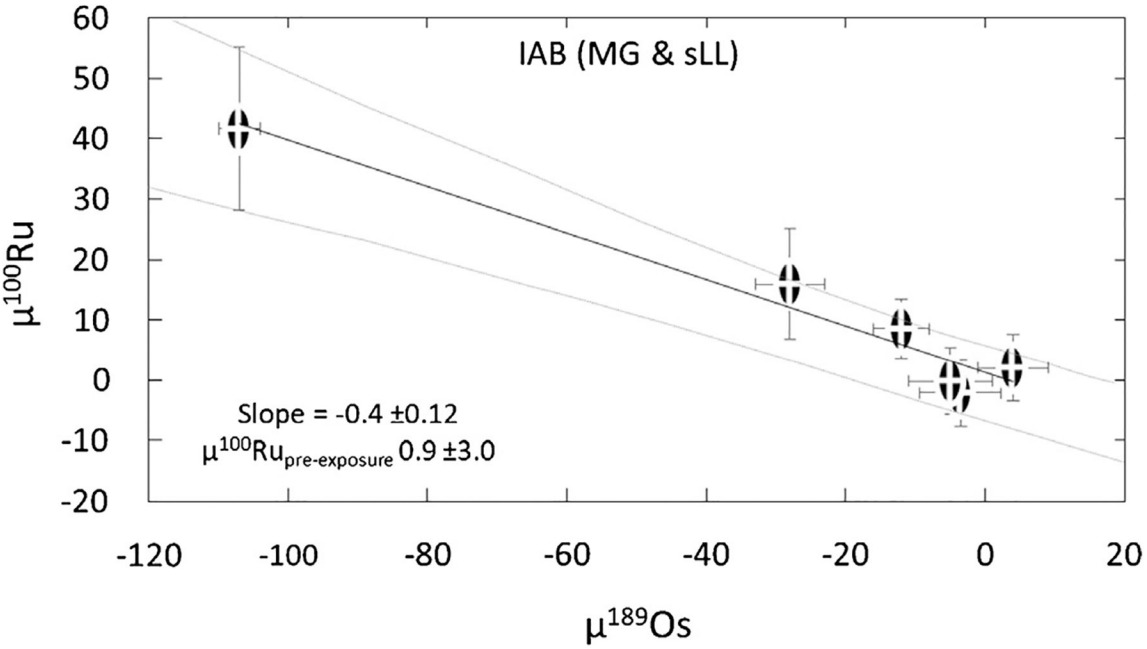

Fig. 2.

μ^{189}Os *vs.* μ^{100} Ru for the lAB complex meteorites (Main Group and sLL subgroup). The dashed line is the linear regression through the meteorite data and the grey lines is the error envelope of the regression, both calculated using ISOPLOT (Ludwig, 2003).

Earth Planet Sci Lett. Author manuscript; available in PMC 2019 April 04.

Table 1

List of samples, locality, $^{187}Os/^{188}Os$ ratios, and Os model ages.

Sample	Sample type	Location	$^{187}Os/^{188}Os$	Os model age	Reference
Terrestrial samples					
Yodda	Os-Ir alloy	Papua New Guinea	0.1290024 ± 12	80 Ma	[1]
Bald Hills	Os-Ir alloy	Tasmania (AU)	0.120041 ± 22	130 Ma	[1]
Savage River	Os-Ir alloy	Tasmania (AU)	0.119940 ± 9	130 Ma	[1]
L5–1	Os-Ir-Ru alloy	Josephine Ophiolite Complex (US)	0.1411853 ± 30	162 Ma	[2]
M3–6	Os-Ir-Ru alloy	Josephine Ophiolite Complex (US)	0.1228417 ± 52	162 Ma	[2]
M8–2	Os-Ir-Ru alloy	Josephine Ophiolite Complex (US)	0.1260988 ± 55	162 Ma	[2]
C1	Chromitite	Shetland Ophiolite Complex (UK)	0.129210 ± 28	492 Ma[a]	[3,4]
C2	Chromitite	Shetland Ophiolite Complex (UK)	0.129227 ± 8	492 Ma[a]	[3,4]
C3	Chromitite	Shetland Ophiolite Complex (UK)	0.129250 ± 6	492 Ma[a]	[3,4]
Guli	Os-Ir alloy	Guli clinopyroxene-dunite massif (RU)	0.12428–0.12478	545–615 Ma	[5]
Kushva	Os-Ir alloy	Urals (RU)	-	870 Ma	[6]
Nizhny Tagil	Os-Ir alloy	Urals (RU)	-	870 Ma	[6]
B-1	Ru-Os-Ir alloy	Witwatersrand (SA)	–	2.66–4.10 Ga	[7]
Meteoritic samples					
Morasko	Iron meteorite	IAB-Main Group	0.14649	3.5 ± 1.3 Ma[b]	[8]
Hope	Iron meteorite	IAB-Main Group	0.16727	-	[8]
Campo del Cielo	Iron meteorite	IAB-Main Group	0.12418	4.1 ± 0.5 Ma[b]	[8]
Bischtübe	Iron meteorite	IAB-sLL	0.12764	4.5 ± 1.2 Ma[b]	[8]
Deport	Iron meteorite	IAB-sLL	0.12870	5.3 ± 2.0 Ma[b]	[8]
Toluca	Iron meteorite	IAB-sLL	0.13228	5.4 ± 1.2 Ma[b]	[8]

[1] Brandon et al. (1998);

[2] Walker et al. (2005);

[3] O'Driscoll et al. (2012);

[4] Spray and Dunning, 1991;

[5] Malitch et al. (2011);

[6] Anikina et al 2014;

[7] Malitch and Merkle (2004);

[8] Worsham et al. (2017).

[a] A zircon U-Pb crystallization age from a plagiogranite vein cutting the upper portion of the SOC providing a minimum age (from Spray and Dunning, 1991)

[b] Metal-silicate Hf-W segregation model ages (Δt_{CAI}) calculated relative to CAI (Worsham et al., 2017).

Table 2

The μ^{100} Ru values for chromitites and Os-Ir-Ru alloys. Data are corrected using the Nier reduction method unless otherwise specified. The uncertainties associated with individual analyses are the internal error (2SE) associated with the measurement, unless there is only one analysis for the sample in which case the uncertainties are the 2SD of the standards measured during the relevant campaign. The uncertainties for sample means, where $n < 3$, are reported as the 2SD of the *Alfa Asear* standard, or the sample, whichever was greater. The uncertainties for sample means, where $n \geq 3$, are the 2SE associated with the multiple measurements of the sample. The uncertainties associated with the IAB iron meteorite group are defined by the extent of the error envelop at μ^{189}Os = 0 for the trend μ^{189}Os *vs.* μ^{100} Ru, obtained using the ISOPLOT program (Ludwig, 2003). The uncertainties associated with the oceanic mantle are an average of the 2SD of repeated analysis of the *Alfa Asear* standard from each measurement campaign.

Location/Sample	μ^{100}Ru	±
SOC (UK)		
C1	4.0	9.0
C2	4.0	9.0
C3_a	−1.4	5.4
C3_b	−0.1	6.8
C3_c	−1.4	2.7
C3_d	1.3	5.4
$C3_{mean}$	−0.4	1.3
JOC (US)		
M3_6	7.4	6.8
M8_02	−4.5	6.8
L5_3_a	2.6	5.8
L5_3_b	−3.7	5.4
L5_3_c	−5.4	6.7
L5_3_d	1.5	3.9
L5_3_e	2.6	8.1
$L5\_3_{mean}$	−0.5	3.4
Witwatersrand (SA)		
B-1_a	0.3*	2.5*
B-1_b	0.4*	3.7*
B-1_c	4.1*	3.3*
B-1_d	1.5*	3.3*
B-1_e	−1.1*	3.0*
B-1_f	−4.4*	3.2*
B-1_g	1.8*	3.4*
$B\text{-}1_{mean}$	0.4*	2.0*
Urals (RU)		
Kushva_a	−4.4	5.1

Location/Sample	μ^{100}Ru	±
Kushva_b	2.4	3.1
Kushva_c	10.0	3.4
Kushva mean	2.7	10.9
Nizhny Tagil_a	14.9	6.3
Nizhny Tagil_b	3.2	5.0
Nizhny Tagil$_{mean}$	9.1	7.5
Guli_a	4.3*	6.5*
Guli_b	−4.8*	4.7*
Guli_c	3.9*	3.5*
Guli_d	2.8*	4.0*
Guli$_{mean}$	1.6*	3.9*
Tasmania (AU)		
Bald Hills	−7.8	8.6
Savage River	−6.8	8.6
Papua New Guinea		
Yodda_a	1.5	3.3
Yodda_b	6.5	3.3
Yodda_c	4.1	4.7
Yodda$_{mean}$	4.1	2.9
IAB (MG,sLL)	0.9	3.0
Oceanic mantle	1.2	7.2

*Data obtained using the measured oxygen reduction scheme.

Table 3

μ^{189}Os and cosmic ray uncorrected μ^{100} Ru for IAB iron meteorites. The uncertainties for multiple analyses of individual samples, where $n < 3$, are reported as the 2SD of the standard, or the sample, whichever was greater. The uncertainties for individual samples, where $n \geq 3$, are the 2SE associated with the multiple measurements of the sample. Where n is the number of analyses of a single sample solution for (a) Ru and (b) Os.

Sample	n^a	μ^{100}Ru	±	n^b	μ^{189}Os	±
IAB Main Group						
Campo del Cielo$_{mean}$	1	2.1	5.6	2	4.0	5.0
Morasko$_{mean}$	3	8.5	4.9	1	−12.0	4.0
Hope	1	−2.1	5.6	3	−3.5	5.9
IAB sLL						
Bischtübe	1	15.9	9.2	3	−28.0	5.0
Deport$_{mean}$	2	41.7	13.5	3	−107.0	3.0
Toluca$_{mean}$	1	−0.2	5.6	4	−5.0	6.0